

Robustness Assessment of a Runway Object Classifier for Safe Aircraft Taxiing

Yizhak Elboher^{1*}, Raya Elsaleh^{1*}, Omri Isac^{1*}, Mélanie Ducoffe², Audrey Galametz², Guillaume Povéda², Ryma Boumazouza², Noémie Cohen², and Guy Katz¹

¹ The Hebrew University of Jerusalem

² Airbus Central Research & Technology, AI Research

Abstract. As deep neural networks (DNNs) are becoming the prominent solution for many computational problems, the aviation industry seeks to explore their potential in alleviating pilot workload and in improving operational safety. However, the use of DNNs in this type of safety-critical applications requires a thorough certification process. This need can be addressed through formal verification, which provides rigorous assurances — e.g., by proving the absence of certain mispredictions. In this case-study paper, we demonstrate this process using an image-classifier DNN currently under development at Airbus and intended for use during the aircraft taxiing phase. We use formal methods to assess this DNN’s robustness to three common image perturbation types: *noise*, *brightness* and *contrast*, and some of their combinations. This process entails multiple invocations of the underlying verifier, which might be computationally expensive; and we therefore propose a method that leverages the monotonicity of these robustness properties, as well as the results of past verification queries, in order to reduce the overall number of verification queries required by nearly 60%. Our results provide an indication of the level of robustness achieved by the DNN classifier under study, and indicate that it is considerably more vulnerable to noise than to brightness or contrast perturbations.

1 Introduction

In recent years, deep neural networks (DNNs) have been revolutionizing computer science, advancing the state of the art in many domains [19] — including natural language processing, computer vision, and many others. In the aviation domain, aircraft manufacturers are now exploring how deep-learning-based technologies could decrease the cognitive load on pilots, while increasing the safety and operational efficiency of, e.g., airports. In particular, these technologies could prove useful during the aircraft taxi phase, which often creates an increased cognitive load on pilots that have to simultaneously manage the flight plan, the aircraft itself, and any objects on the tarmac.

* Authors contributed equally.

Despite their success, DNNs are known to be prone to various errors. Notably among these are *adversarial inputs* [6], which are small input perturbations that lead to incorrect and potentially unsafe DNN outputs. While there exist many techniques for efficiently finding adversarial inputs, it is unclear how to certify that no such examples exist. However, such certification is required to allow the integration of DNNs into safety-critical industrial systems, e.g., in aviation.

One promising approach for addressing this need is by *formally verifying* the correctness of DNNs [3, 10]. Typically, DNN verification tools seek to prove that, for a given infinite set of inputs, a DNN only produces outputs that fall within a safe subspace of outputs. Although DNN verification has been making great strides [1, 7, 8, 9, 14, 15, 16, 17, 18, 20], it has only been applied to a handful of real-world systems.

In this case-study paper, we study the applicability and scalability of DNN verification through an object classification use-case, relevant to the aviation domain and of specific interest to Airbus. We explore pertinent vision-oriented perturbations (*noise*, *brightness*, and *contrast*) and use formal verification to quantify their effects on DNN’s robustness. As a back-end engine, we use the Marabou DNN verifier [13]. We also demonstrate that the verification process can be optimised by leveraging the monotonicity of the studied perturbations.

Our results indicate that while the DNN is highly sensitive to noise perturbations, it is slightly less vulnerable to contrast and brightness perturbations. This is a reassuring result, as these perturbations are strongly correlated with highly unpredictable operating conditions, especially outdoors. More broadly, our results showcase the usefulness and potential of DNN verification in aviation that could easily be extended to other safety-critical domains.

2 Background

Deep Neural Networks. A deep neural network [5] $\mathcal{N} : \mathbb{R}^n \rightarrow \mathbb{R}^k$ is comprised of m layers, L_1, \dots, L_m . Each layer L_i consists of a set of nodes, S_i . When \mathcal{N} is evaluated, each node in the input layer is assigned an initial value. Then, the value of the j^{th} node in the $2 \leq i < m$ layer, v_j^i , is computed as:

$$v_j^i = f \left(\sum_{l=1}^{|S_{i-1}|} w_{j,l}^{i-1} \cdot v_l^{i-1} + b_j^i \right)$$

where $f : \mathbb{R} \rightarrow \mathbb{R}$ is an *activation function* and $w_{j,l}^{i-1}, b_j^i \in \mathbb{R}$ are the respective *weights* and *biases* of \mathcal{N} . The most common activation function is the *rectified linear unit*, defined as $\text{ReLU}(x) = \max(0, x)$. Finally, neurons in the output layer are assigned values using an affine combination only. The output of the DNN is the values of the nodes in its final layer. An image-classifier $\mathcal{N} : \mathbb{R}^n \rightarrow C \subset \mathbb{N}$ assigns each input image x' a class $c \in C$, which described the main object depicted in x' . For convenience, x' is regarded as both a vector and a matrix, interchangeably. For an example of a DNN and its evaluation, see Appendix B.

DNN Verification. For a DNN $\mathcal{N} : \mathbb{R}^n \rightarrow \mathbb{R}^k$, input property $P \subset \mathbb{R}^n$ and output property $Q \subset \mathbb{R}^k$, the *DNN verification problem* is to decide whether there exist $x \in P$ and $y \in Q$ such that $\mathcal{N}(x) = y$. If such a pair exists, the verification query (\mathcal{N}, P, Q) is *satisfiable* (SAT), and the pair (x, y) is called a witness; otherwise, it is *unsatisfiable* (UNSAT). Typically, Q encodes an undesired behavior, and so a witness is a *counterexample* that demonstrates an error.

3 Industrial Use Case: Runway Object Classification

3.1 Runway Object Classification

In 2020, Airbus concluded its Autonomous Taxi, Take-Off and Landing (ATTOL) project.³ The objective of ATTOL was to design a fully autonomous controller for the taxi, take-off, approach and landing phases of a commercial aircraft — by leveraging state-of-the-art technology, and in particular deep-learning models used for vision-assisted functions. As part of the project, 400 flights over a period of two years were instrumented to collect video data from aircraft in operation. This unique dataset is currently being used to further mature a number of vision-based functions within Airbus. Using this dataset, it was observed that the taxi phase of the flight, in particular, could benefit from autonomous support. During this phase, pilots are conducting aircraft operations, while simultaneously dealing with the unpredictable nature of airport management and traffic. Object identification, in particular of potential threats on the runway, could thus support the pilots during this phase; and indeed, a number of object classifiers are being tested for this purpose within Airbus.

In this study, we focus on images of runway objects extracted from taxiing videos i.e., all objects are observed from an aircraft on ground. We extract (224×224) pixel images from the original, high-resolution gray-scaled images, centered on a specific runway object. A DNN N_1 is trained on resampled (32×32) images. The four considered classes are *Aircraft*, *Vehicle*, *Person*, and *Negative*, extracted where no object is found. N_1 is a feedforward DNN, with roughly 8000 ReLU neurons, and an accuracy of 85.3% on the test dataset (1145/1342 images).⁴

3.2 Properties of Interest

We seek to verify the *local robustness* of a runway object classifier \mathcal{N} ; i.e., that small perturbations around a correctly-classified input x' do not cause misclassification, encoded by Q . We specify Q as: $Q_{x'} := C \setminus \mathcal{N}(x')$. We use the input property P to define three perturbation types: noise, brightness and contrast.

Noise. In this widely studied form of perturbation [2, 12], the perturbed input images are taken from an ϵ -ball around x' : $P = B_\epsilon(x')$, where B_ϵ is the ℓ_∞ - ϵ -ball around x' , and $\epsilon > 0$.

³ <https://www.airbus.com/en/newsroom/press-releases/2020-06-airbus-concludes-attol-with-fully-autonomous-flight-tests>

⁴ This DNN is not intended for real-life applications. More robust models are currently under development, in part supported by analyses such as the one presented here.

Brightness. A brightness perturbation is caused by the shifting of all pixels of x' by a constant value b : $bright(\alpha, b) := \alpha + b \cdot J_n$, where J_n is the all-ones matrix of size $n \times n$. We define $P = bright_\beta(\alpha) := \{bright(\alpha, b) \mid |b| \leq \beta\}$ for some $\beta > 0$, to allow all brightness perturbations of absolute value at most β . See Appendix A for a visual example.

Contrast. A contrast perturbation $con(\alpha, c, \mu)$ is created by scaling all image pixels multiplicatively, rescaling their difference from a mean value $\mu \in [0, 1]$ by a multiplicative constant $c \in \mathbb{R}_{\geq 0}$: $con(x', c, \mu) := \mu \cdot J_n + c \cdot (x' - \mu \cdot J_n)$. We then set $P = con_{\gamma, \mu}(x') := \{con(x', c, \mu) \mid |c - 1| \leq \gamma\}$, to encode all contrast perturbations with value of at most γ , where μ remains constant and $\gamma \in [0, 1]$. See Appendix A for a visual example.

4 The Formal Verification Process

4.1 Encoding Brightness and Contrast Perturbations

We now show how to encode the brightness and contrast properties described in Section 2 into verification queries that assess robustness to noise perturbations over a modified input space. This reduction allows us to use any of the available tools that support such queries as a backend. The encoding is performed by adding a new input layer to the network, as illustrated in Fig. 1.

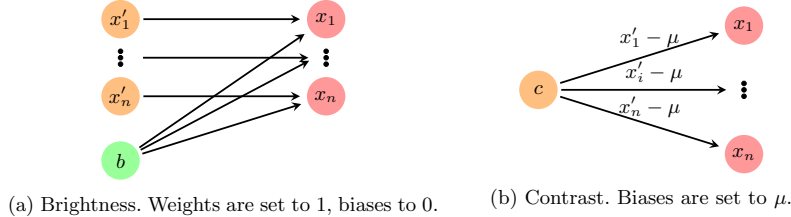


Fig. 1: Modeling brightness and contrast perturbations by adding an input layer.

Brightness. The new input layer clones the original input layer, and adds a single neuron b to represent the brightness perturbations. The weights from the new layer to the following, original input layer are set to 1, so that every variable $x_i \in x$ is assigned $x_i = x'_i + b$. The bounds for the new neuron are set to $b \leq \beta, b \geq -\beta$, whereas inputs x'_i are exactly restricted to the input around which the robustness is being verified. We note that in this case, this single construction allows the verification of the robustness around any input, by selecting appropriate x'_i values. We further note that this construction can be used to simultaneously encode noise and brightness perturbations, by bounding the input neurons x'_i to an ϵ -ball around an input of interest. This gives rise to two-dimensional queries, for any combination of β and ϵ values, which allows to model a more realistic nature of perturbations.

Contrast. The new input layer contains a single input neuron, c . We treat μ, x' as constants, and set the weights from the new layer in a way that every neuron x_i in that layer is assigned $x_i = (x'_i - \mu) \cdot c + \mu$. Finally, we set the bounds $c \geq 1 - \gamma, c \leq 1 + \gamma$. We note that the contrast perturbation is multiplicative with respect to c, μ , and the input image x' . Since DNN verification algorithms typically only support linear operations, either x' or c should be fixed. Therefore, a separate DNN is constructed for each input image; and there is no immediate way to encode a simultaneous noise perturbation.

4.2 Incremental Verification Algorithm

For any fixed image x' , we seek to generate numerous brightness, noise and contrast robustness queries, with different values of ϵ, β and γ . Since executing these queries is computationally expensive, we exploit the monotonicity of these properties to reduce their number. Let $\beta' < \beta, \epsilon' < \epsilon$ and $\gamma' < \gamma$. If there exists an adversarial example for parameters β', ϵ' or γ' , it then also constitutes a counterexample for a query with parameters β, ϵ or γ respectively. Conversely, if the network is robust with respect to parameters β, ϵ or γ , then it is also robust to perturbation with parameters β', ϵ' or γ' respectively.

We exploit this property in a binary search algorithm for contrast queries, and in our *incremental verification algorithm* for brightness and noise queries. The incremental verification algorithm initializes a grid representing all combinations of ϵ, β parameters that need to be verified. It is described and illustrated in Appendix C. The algorithm iteratively calls the verifier to solve a query and, based on the verifier's output, deduces the results of either a column or a row of the grid. For brightness and noise queries, this represents $O(m)$ calls to the verifier instead of $O(m^2)$, where m is the number of possible values of β or ϵ (the maximal of the two). For contrast queries, it allows the use of a logarithmic number of invocations of the verifier instead of a linear number.

5 Evaluation

For the 1145 correctly classified test images, we verify N_1 's robustness to noise and brightness for parameters $(\epsilon, \beta) \in [0, 0.05, 0.1, 0.15, 0.2] \times [0, 0.1, 0.2, 0.3, 0.4, 0.5]$, and to contrast perturbations with mean pixel value $\mu = 0.2585$ and $\gamma \in [0.1, 0.2, \dots, 0.9]$. We make use the incremental verification algorithm for noise and brightness perturbations. For contrast, we ran a binary search algorithm to find the minimal γ parameter for which the query is UNSAT. We use an arbitrary timeout of 22.5K seconds per single query, and 80 hours for the overall runtime to analyze a single input point. The results are summarised below and in Appendix D.

Fig. 2 shows the percentage of UNSAT queries for noise and brightness perturbations, indicating the absence of counter examples, of 1097 points for which the analysis has not timed out. The incremental verification algorithm invoked the verifier on 13231 queries, whereas the results of 59% of the queries were

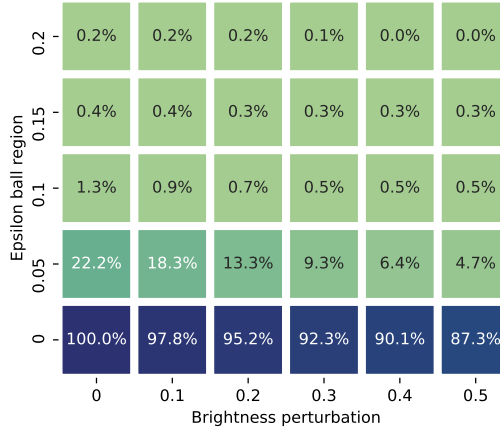


Fig. 2: Percentage of UNSAT queries per noise and brightness parameters. deduced, using the incremental approach, without additional invocations. Fig. 3 shows the percentage of UNSAT queries for contrast perturbations within the range $[1 - \gamma, 1 + \gamma]$. The binary search algorithm invoked the verifier 3915 times, whereas the remaining 62% of the queries were deduced without additional invocations.

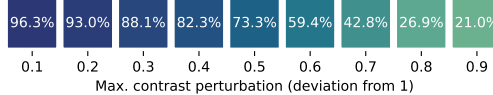


Fig. 3: Percentage of UNSAT queries per contrast parameter

Overall, the results indicate that the classifier shows similar robustness to contrast and brightness perturbations. However, it is significantly more sensitive to noise perturbations. We note that noise in images comes from various sources. Some are inherent to the camera's sensor (e.g., impulse noise, thermal noise) and/or associated electronics (e.g. shot noise). Others are direct consequences of operating and environmental conditions (e.g., low-light conditions, scenery's colors etc.). Brightness and contrast also fall into this category; they are both inherently related to operating conditions. Although noise originated from image acquisition is certainly a nuisance, it can in part be reduced by noise reduction techniques as well as an expert understanding of the camera characteristics and continuous quality tracking. The latter is more challenging to predict or mitigate as operating conditions (weather, time of day, scenery, etc.) are almost endless. It is therefore somehow reassuring that our classifier seems to be less vulnerable to contrast and brightness, as these perturbations are highly unpredictable.

6 Conclusion

In this work, we assessed the robustness of a prototype runway object classifier provided by Airbus, with respect to three image perturbations. Moving forward, we aim to assess additional Airbus networks, and to verify their robustness to simultaneous robustness and contrast perturbations. In addition, we aspire to increase the reliability of the results by using the *proof producing* version of Marabou [11]. To improve performance, we intend to examine applying DNN abstraction methods [4] to the verification queries we have used.

Acknowledgements. This research was partially funded by Airbus Central Research & Technology, AI Research.

References

- [1] Brix, C., Müller, M., Bak, S., Johnson, T., Liu, C.: First Three Years of the International Verification of Neural Networks Competition (VNN-COMP). *Int. Journal on Software Tools for Technology Transfer* pp. 1–11 (2023)
- [2] Casadio, M., Komendantskaya, E., Daggitt, M., Kokke, W., Katz, G., Amir, G., Refaeli, I.: Neural Network Robustness as a Verification Property: A Principled Case Study. In: Proc. 34th Int. Conf. on Computer Aided Verification (CAV). pp. 219–231 (2022)
- [3] Cheng, C.H., Diehl, F., Hinz, G., Hamza, Y., Nührenberg, G., Rickert, M., Ruess, H., Truong-Le, M.: Neural Networks for Safety-Critical Applications—Challenges, Experiments and Perspectives. In: Proc. Design, Automation & Test in Europe Conf. & Exhibition (DATE). pp. 1005–1006 (2018)
- [4] Elboher, Y., Gottschlich, J., Katz, G.: An Abstraction-Based Framework for Neural Network Verification. In: Proc. 32nd Int. Conf. on Computer Aided Verification (CAV). pp. 43–65 (2020)
- [5] Goodfellow, I., Bengio, Y., Courville, A.: Deep Learning. MIT Press (2016)
- [6] Goodfellow, I., Shlens, J., Szegedy, C.: Explaining and Harnessing Adversarial Examples (2014), technical Report. <http://arxiv.org/abs/1412.6572>
- [7] Gopinath, D., Katz, G., Păsăreanu, C., Barrett, C.: DeepSafe: A Data-driven Approach for Assessing Robustness of Neural Networks. In: Proc. 16th. Int. Symposium on Automated Technology for Verification and Analysis (ATVA). pp. 3–19 (2018)
- [8] Henriksen, P., Lomuscio, A.: Efficient Neural Network Verification via Adaptive Refinement and Adversarial Search. In: Proc. 24th European Conf. on Artificial Intelligence (ECAI). pp. 2513–2520 (2020)
- [9] Huang, X., Kwiatkowska, M., Wang, S., Wu, M.: Safety Verification of Deep Neural Networks. In: Proc. 29th Int. Conf. on Computer Aided Verification (CAV). pp. 3–29 (2017)
- [10] Huang, X., Kroening, D., Ruan, W., Sharp, J., Sun, Y., Thamo, E., Wu, M., Yi, X.: A Survey of Safety and Trustworthiness of Deep Neural Networks: Verification, Testing, Adversarial Attack and Defence, and Interpretability. *Computer Science Review* 37 (2020)

- [11] Isac, O., Barrett, C., Zhang, M., Katz, G.: Neural Network Verification with Proof Production. In: Proc. 22nd Int. Conf. on Formal Methods in Computer-Aided Design (FMCAD). pp. 38–48 (2022)
- [12] Katz, G., Barrett, C., Dill, D., Julian, K., Kochenderfer, M.: Reluplex: a Calculus for Reasoning about Deep Neural Networks. Formal Methods in System Design (FMSD) (2021)
- [13] Katz, G., Huang, D., Ibeling, D., Julian, K., Lazarus, C., Lim, R., Shah, P., Thakoor, S., Wu, H., Zeljić, A., Dill, D., Kochenderfer, M., Barrett, C.: The Marabou Framework for Verification and Analysis of Deep Neural Networks. In: Proc. 31st Int. Conf. on Computer Aided Verification (CAV). pp. 443–452 (2019)
- [14] Lyu, Z., Ko, C.Y., Kong, Z., Wong, N., Lin, D., Daniel, L.: Fastened Crown: Tightened Neural Network Robustness Certificates. In: Proc. 34th AAAI Conf. on Artificial Intelligence (AAAI). pp. 5037–5044 (2020)
- [15] Mangal, R., Nori, A., Orso, A.: Robustness of Neural Networks: A Probabilistic and Practical Approach. In: Proc. IEEE/ACM 41st Int. Conf. on Software Engineering: New Ideas and Emerging Results (ICSE-NIER). pp. 93–96 (2019)
- [16] Müller, M., Makarchuk, G., Singh, G., Püschel, M., Vechev, M.: PRIMA: General and Precise Neural Network Certification via Scalable Convex Hull Approximations. In: Proc. 49th ACM SIGPLAN Symposium on Principles of Programming Languages (POPL) (2022)
- [17] Ostrovsky, M., Barrett, C., Katz, G.: An Abstraction-Refinement Approach to Verifying Convolutional Neural Networks. In: Proc. 20th. Int. Symposium on Automated Technology for Verification and Analysis (ATVA). pp. 391–396 (2022)
- [18] Singh, G., Gehr, T., Puschel, M., Vechev, M.: An Abstract Domain for Certifying Neural Networks. In: Proc. 46th ACM SIGPLAN Symposium on Principles of Programming Languages (POPL) (2019)
- [19] Szegedy, C., Toshev, A., Erhan, D.: Deep Neural Networks for Object Detection. Advances in Neural Information Processing Systems 26 (2013)
- [20] Wu, H., Zeljić, A., Katz, G., Barrett, C.: Efficient Neural Network Analysis with Sum-of-Infeasibilities. In: Proc. 28th Int. Conf. on Tools and Algorithms for the Construction and Analysis of Systems (TACAS). pp. 143–163 (2022)

Appendix

A Visualization of Brightness and Contrast Perturbations

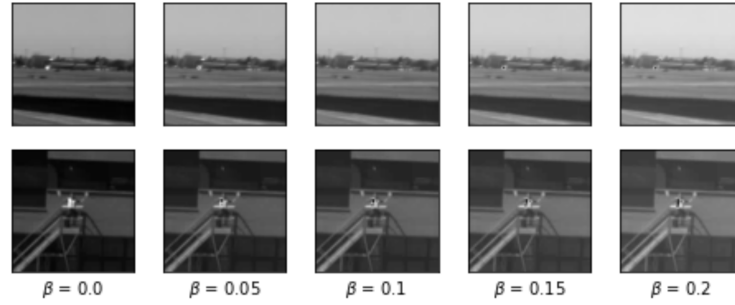


Fig. 4: Brightness perturbations for an ‘Aircraft’ and a ‘Person’ from the test set.

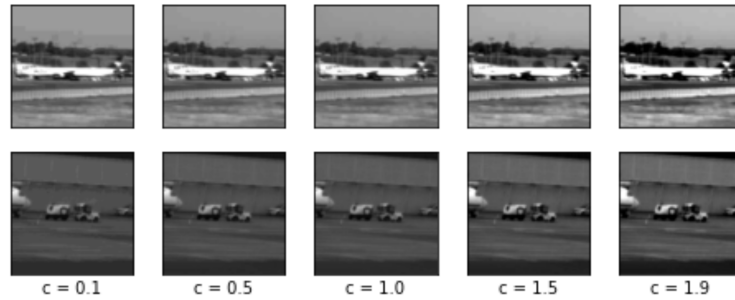


Fig. 5: Contrast perturbations for an ‘Aircraft’ and a ‘Vehicle’ from the test set.

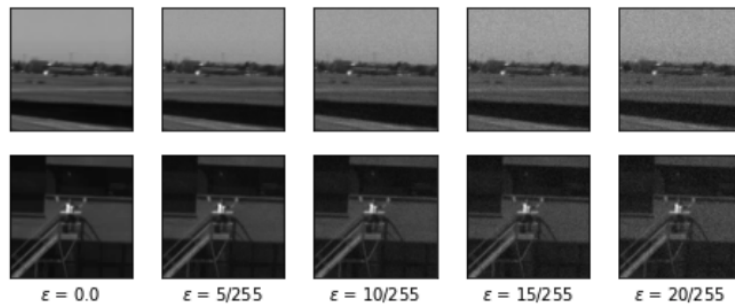


Fig. 6: Levels of l_{∞} -norm bounded perturbations for an ‘Aircraft’ and a ‘Vehicle’.

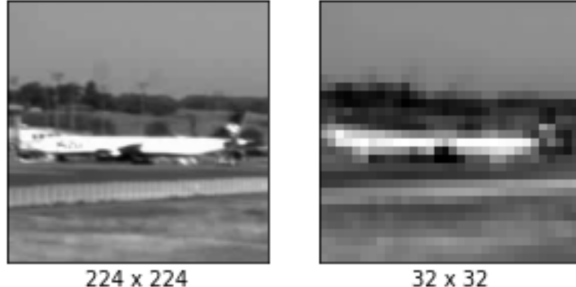


Fig. 7: Illustration of an ‘Aircraft’ image at different resolutions.

B An Example of DNN

Consider the DNN with 4 layers that appears in Fig. 8, where all biases are set to zero and are ignored. For input $\langle 2, -1 \rangle$, the first node in the second layer evaluates to $\text{ReLU}(2 \cdot 1.5 + -1 \cdot (-1)) = \text{ReLU}(4) = 4$; and the second node in the second layer evaluates to $\text{ReLU}(2 \cdot -1) = \text{ReLU}(-2) = 0$; Then the node in the third layer evaluates to $\text{ReLU}(4 - 0) = 4$. and thus the output of the network is 2.

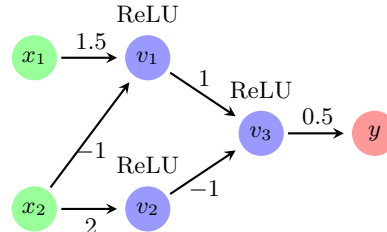


Fig. 8: A toy DNN.

C Incremental Verification Algorithm

In this appendix, we provide a description and the pseudo-code for the incremental verification algorithm described in Section 4. We then provide an example that demonstrates a run of the algorithm over a grid of 4×5 , representing 5 different values of β and 4 of ϵ .

For intuition, consider a discrete two-dimensional grid, where each cell represents a tuple of the query’s parameters. The observation in Section 4.2 states that for every row and every column, there is at most one transition from `UNSAT`

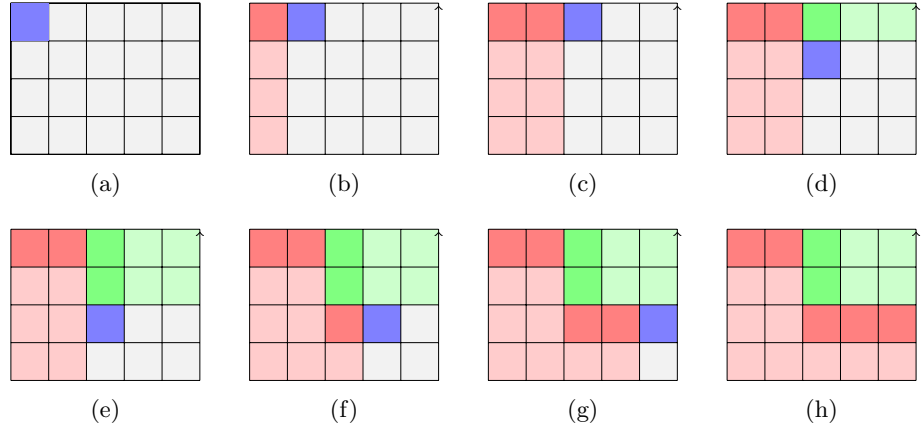


Fig. 9: Demonstration of the algorithm's run.

to **SAT**. This transition is represented by a step graph within the grid, with size $O(m)$ cells, where $m = \max(\text{width}, \text{height})$ (see Fig. 9). Starting from a corner, the algorithm explores a single cell in the step graph on each iteration.

The algorithm assumes the existence of a verification procedure $\text{verify}(\mathcal{N}, x', \beta, \epsilon)$ which verifies the robustness of a network \mathcal{N} to noise perturbations of value at most ϵ and brightness perturbations of value at most β around an image x' . The algorithm is given an input network \mathcal{N} , an image α , and two increasingly ordered arrays B, E , containing the values of parameters β and ϵ we intend to check, respectively. Intuitively, the algorithm initializes a grid representing all possible combinations of parameters $(\beta, \epsilon) \in B \times E$, and a temporary tuple (b, e) representing the lowest value of β and highest value ϵ and corresponding to the top-left corner of the grid. The algorithm then iteratively calls the $\text{verify}(\mathcal{N}, x', b, e)$ procedure to populate the grid. If the result is **SAT**, then for all queries with the same ϵ value, and a greater β (all cells to the right of the current cell) the result is **SAT** as well.⁵ We then mark the relevant cells with **SAT** and decrement ϵ to the next value. If the result is **UNSAT**, then for all queries with the same β value, and a smaller ϵ (all cells to the bottom of the current cell), the result is **UNSAT** as well. We then mark the relevant cells with **UNSAT** and increment β to the next value. When the current cell reaches the final column or row, then a usual binary search algorithm is used to find the remaining results.

In order to support the use of real-world verifiers, we handle cases of **TIMEOUT**, or errors as well. When these cases occur, we mark the corresponding cell (e, b) with an **UNKNOWN** result, and increment the value of b as if the results was **SAT**. In addition, we use binary search for the remaining values of e , were the value of b is constant.

⁵ Note that this is the case for all queries with greater values of ϵ, β (the top right rectangle), though the values of queries with a greater ϵ value are already decided. A dual argument applies to the **UNSAT** case as well.

In Fig. 9, the grid represents the options for verification queries of robustness for brightness and noise perturbation, with parameters $(\beta, \epsilon) \in [0.1, 0.2, 0.3, 0.4, 0.5] \times [0.1, 0.2, 0.3, 0.4]$. The purple cell represents the current tuple (β, ϵ) . Red marks **UNSAT** queries, green marks **SAT** queries. Rich colors represent a call for the verifier, pale colors represent a deduction of satisfiability.

The algorithm first queries the verifier to verify robustness with parameters $(0.4, 0.1)$, which returns **UNSAT**. Then, the algorithm deduces **UNSAT** for queries with $\beta = 0.1, \epsilon < 0.4$ without calling the verifier again, and queries the verifier to verify robustness with parameters $(0.4, 0.2)$. Since the verifier returns **UNSAT** again, the algorithm deduces **UNSAT** for queries with $\beta = 0.2, \epsilon < 0.4$ and queries the verifier to verify robustness with parameters $(0.4, 0.3)$. This time, the verifier returns **SAT**, so the algorithm deduces **SAT** for queries with $\beta > 0.2, \epsilon = 0.4$. The algorithm then queries the verifier to verify robustness with parameters $(0.3, 0.3)$. The rest of the iterations continue in a similar manner.

Algorithm 1 Incremental verification algorithm

Input: Arrays B, E with values of ϵ, β in increasing order, respectively, a verifier V , a network \mathcal{N} and an image x' .

Output: A grid representing the robustness of \mathcal{N} to brightness and noise perturbations around x' , for all values in B, E .

```

 $b \leftarrow 0$ 
 $e \leftarrow \text{length}(E) - 1$ 
 $grid \leftarrow 0_{\text{length}(E) \times \text{length}(B)}$ 
while  $b < \text{length}(B)$  and  $e \geq 0$  do
    if  $b = \text{length}(B) - 1$  then
        Binary search with remaining values of  $e$ ;  $b$  is constant.
    end if
    if  $e = 0$  then
        Binary search with remaining values of  $b$ ;  $e$  is constant.
    end if
     $result \leftarrow V.\text{verify}(\mathcal{N}, x', E[e], B[b])$ 
    if  $result = \text{SAT}$  then
         $\forall i \geq b : grid[i][e] \leftarrow \text{SAT}$ 
         $e \leftarrow e - 1$ 
    else if  $result = \text{UNSAT}$  then
         $\forall j \leq e : grid[b][j] \leftarrow \text{UNSAT}$ 
         $b \leftarrow b + 1$ 
    else ▷ Timeout, Memoryout, etc.
         $grid[b][e] \leftarrow \text{UNKNOWN}$ 
        Binary search with remaining values of  $e$ ;  $b$  is constant.
         $b \leftarrow b + 1$ 
    end if
end while
return  $grid$ 

```

D Detailed Evaluation Results

In this appendix, we provide a detailed description of our experiments' results, as described in Section 5.

Result	0.1	0.2	0.3	0.4	0.5	0.6	0.7	0.8	0.9
SAT	20.36	20.57	21.44	25.32	54.26	28.36	27.28	37.41	36.37
UNSAT	19.06	19.06	21.93	106.14	29.37	284.44	241.34	87.12	63.89
UNKNOWN	0	0	0	0	0	0	51.77	59.21	55.07

Table 1: Avg. solving time for contrast queries (sec.).

#	Bright. Noise	0	0.1	0.2	0.3	0.4	0.5
SAT	0	N/A	49.52	61.47	45.09	53.15	66.37
UNSAT		N/A	79.62	73.36	69.92	74.94	83.97
SAT	0.05	50.99	38.27	46.42	373.89	1457.50	1125.45
UNSAT		315.12	423.99	787.40	1111.39	652.05	759.83
SAT	0.1	51.24	48.28	34.85	39.99	422.11	112.02
UNSAT		1887.37	2027.04	159.66	72.11	89.05	301.96
SAT	0.15	39.44	33.46	1474.75	745.56	26.68	22.13
UNSAT		2359.39	225.52	84.77	393.32	259.87	1026.77
SAT	0.2	35.63	18.64	N/A	18.61	N/A	N/A
UNSAT		77.30	92.12	1165.06	1489.30	N/A	N/A

Table 2: Avg. solving time for noise and brightness queries (sec.).

# Queries	0.1	0.2	0.3	0.4	0.5	0.6	0.7	0.8	0.9
SAT Overall	42	80	136	203	306	465	654	836	901
deduced	0	0	80	136	0	326	306	654	836
verified	42	80	56	67	306	159	348	182	65
UNSAT Overall	1103	1065	1009	942	839	680	490	308	241
deduced	1065	839	839	839	0	490	0	0	0
verified	38	226	170	103	839	190	490	308	241
UNKNOWN	0	0	0	0	0	0	1	1	3

Table 3: Results summary for contrast queries.

#	Bright. Noise	0	0.1	0.2	0.3	0.4	0.5
SAT Overall	0	0	24	53	84	109	139
		0	0	0	53	53	109
		0	24	53	31	56	30
UNSAT Overall		1097	1073	1044	1013	988	958
		1097	1044	235	889	67	51
		0	29	809	124	921	907
SAT Overall	0.05	325	371	424	484	533	1093
		0	325	371	325	483	533
		325	46	53	159	50	560
UNSAT Overall		235	194	146	100	69	52
		14	10	8	6	6	3
		221	184	136	94	63	49
SAT Overall	0.1	829	859	884	900	934	936
		0	829	859	829	900	934
		829	30	25	71	34	2
UNSAT Overall		14	10	8	6	6	6
		4	4	3	3	3	0
		10	6	5	3	3	6
SAT Overall	0.15	1036	1045	1054	1064	1070	1075
		0	1036	1047	1036	1064	1070
		1036	11	7	28	6	5
UNSAT Overall		4	4	3	3	3	3
		2	1	1	1	0	0
		2	3	2	2	3	3
SAT Overall	0.2	1087	1091	1091	1091	1091	1091
		0	1087	1091	1087	1091	1091
		1087	4	0	4	0	0
UNSAT Overall		2	1	2	1	0	0
		0	0	0	0	0	0
		2	1	2	1	0	0

Table 4: Summary of results for noise and brightness queries (excluding time-outs).

E The Network is more Robust to Brightness Perturbations than to Noise

In both Fig. 10 and Fig. 11, we show the percentage of the verification queries that had an UNSAT result with respect to certain brightness and noise perturbations. In Fig. 10, we notice that changes in the brightness perturbation parameter β have a minor effect on the queries' answers. On the other hand, as emphasized in Fig. 11, changes in the noise perturbation parameter dramatically decrease the network's performance. This observation tells us that the network is more robust and handles brightness perturbations better than noise.

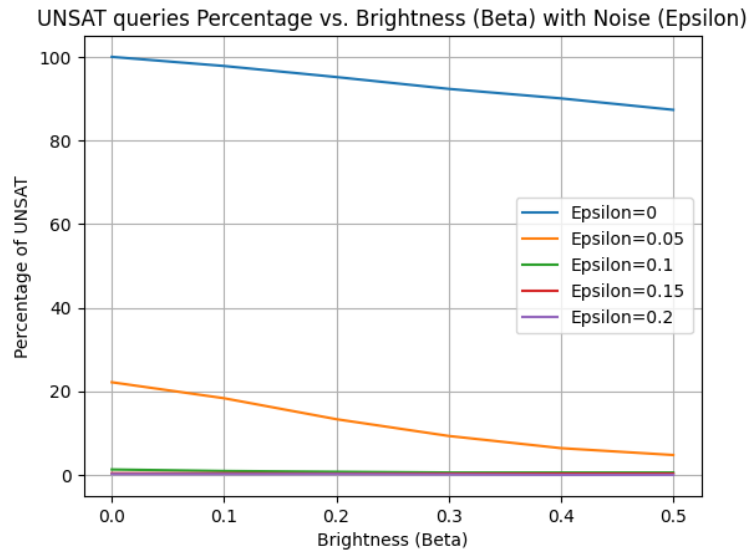


Fig. 10: Percentage of queries with UNSAT answer with respect to different brightness perturbations for every noise perturbation.

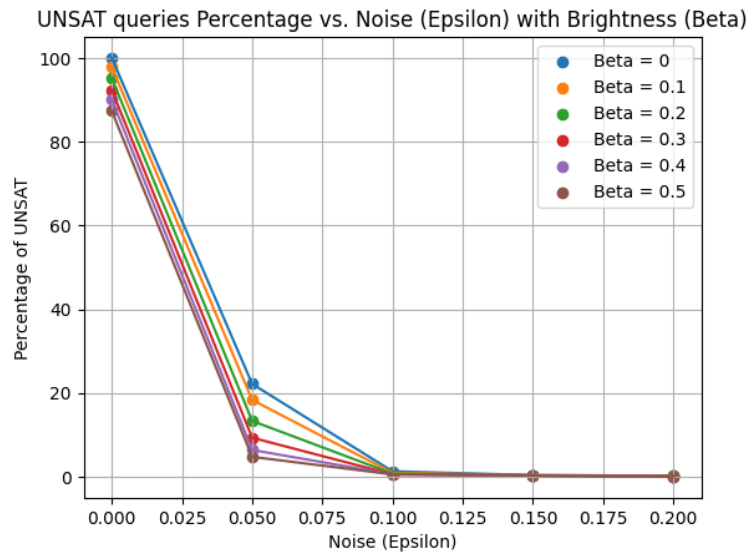


Fig. 11: Percentage of queries with UNSAT answer with respect to different noise perturbations for every brightness perturbation.